Thermal shock behavior of potassium doped and rhenium added tungsten alloys

S Nogami<sup>a</sup>, G Pintsuk<sup>b</sup>, K Matsui<sup>a</sup>, S Watanabe<sup>a</sup>, M Wirtz<sup>b</sup>, T Loewenhoff<sup>b</sup>, and A Hasegawa<sup>a</sup>

<sup>a</sup>Department of Quantum Science and Energy Engineering, Graduate School of Engineering,

Tohoku University, Sendai 980-8579, Japan

<sup>b</sup>Forschungszentrum Jülich GmbH, Institute for Energy and Climate Research, 52425 Jülich,

Germany

E-mail: shuhei.nogami@qse.tohoku.ac.jp

Abstract

High ductile-to-brittle transition temperature (DBTT), recrystallization-induced embrittlement,

and neutron-irradiation-induced embrittlement are potential drawbacks related to the mechanical

properties of tungsten (W) for plasma facing materials (PFMs) of fusion reactor divertors. To

improve the mechanical properties, resistance to recrystallization and neutron irradiation, W

materials modified by potassium (K) doping and alloying by rhenium (Re) have been developed.

In this paper, thermal shock behaviors of these W materials under high heat flux tests were

investigated, which simulated an edge localized mode (ELM) of plasma occurring in fusion

reactors as a transient event. The thermal shock tests were performed with an electron beam

facility, JUDITH 1, and the post-mortem analyses to evaluate the damage caused by the thermal

shock tests were carried out.

**Keywords:** tungsten, potassium doping, rhenium addition, thermal shock, crack formation

## 1. Introduction

Divertor, which has a removal function of waste materials from fusion plasma, is one of the most important components to realize nuclear fusion power reactor. Plasma facing materials (PFMs) of fusion reactor divertor will be suffered by the steady state and transient heat loads. The flux of steady state heat load in divertor will reach to 10–20 MW/m². In addition to these steady state heat loads, the transient event like edge localized modes (ELMs) with power densities of GW/m² will affect the PFMs. As a result of these heat load events, degradation of structural strength and lifetime of divertors could occur due to surface modification, cracking, deformation, and melting of PFMs [1–3]. To evaluate the effects of transient loads in fusion reactor, simulation experiments have been performed using various types of facilities, e.g., plasma gun facilities like QSPA Kh-50 [4], linear plasma generators like MAGNUM-PSI [5], and electron beam test facilities like JUDITH 1 [6] and JUDITH 2 [7].

Pure tungsten (W) is a primary candidate for the PFMs of divertor of ITER and DEMO because of its high melting point, thermal conductivity, sputtering resistance, and low tritium retention. However, there remain some drawbacks related to the mechanical properties, e.g., high ductile-to-brittle transition temperature (DBTT), recrystallization-induced embrittlement, and neutron-irradiation-induced embrittlement. To solve these issues, various W materials have been developed, which were modified by grain refining [8], work hardening [9], alloying [10], and dispersion strengthening [11]. In addition, W-based composites (W fiber reinforced W matrix composites [12] and W foil laminated composites [13] etc.) have also been developed to improve ductility and to produce pseudo ductility. In our previous studies [14–20], W materials (plates or rods) fabricated by powder metallurgy and hot-rolling or swaging have been developed, which were modified by potassium (K) doping and alloying by rhenium (Re) to improve mechanical properties, resistance to recrystallization and neutron irradiation. As consequences, improvement of tensile properties, DBTT, low cycle fatigue life, and recrystallization temperature, and suppression of irradiation hardening have been clarified. In contrast, decrease in melting point (approximately 3200 °C in W-5%Re) and thermal conductivity (approximately 10% reduction in W-3%Re [21]) are known as negative effects of alloying by Re for the application of PFMs.

Because the performance (structural strength and lifetime etc.) of PFMs under fusion reactor environment are not determined by the individual material properties but by their synergistic effects, the high heat flux tests are expected to clarify the effectiveness of the modified W materials for PFMs. Thermal shock behaviors under ELM-like heat load of the W materials modified by K-doping and alloying by Re were investigated in the present study.

## 2. Experimental

Pure W, K-doped W, W-3%Re, and K-doped W-3%Re plates with a thickness of 7 mm

fabricated by powder metallurgy and hot-rolling and K-doped W rod with a diameter of 20 mm fabricated by powder metallurgy and swaging were examined in the present study. A final heat treatment of all materials was carried out at 900 °C for stress relief. The concentration of K in the K-doped W materials was approximately 30 ppm. All materials were prepared in the as-received condition, which are condition after the hot-rolling/swaging and stress relief heat treatment. In addition, only pure W and K-doped W-3%Re plates were prepared in the recrystallized condition, which are condition after the heat treatment at 2300 °C for 1 h. The major chemical composition, heat treatment condition, abbreviation of material name, grain size [14–20], recrystallization temperature [16], tensile strength [18, 19], DBTT by tensile test [18, 19], and inverse pole figure (IPF) images obtained by an electron backscatter diffraction (EBSD) of materials evaluated in the present study are summarized in table 1.

The thermal shock tests were performed with an electron beam irradiation facility, JUDITH 1, at Forschungszentrum Jülich, Germany [6]. Absorbed power densities, base temperature, pulse duration, and pulse numbers of this tests were 0.19 and 0.38 GW/m<sup>2</sup>, 1000 °C, 1 ms, and 1000 cycles, respectively. For the thermal shock tests, specimens were prepared to a shape with 5 mm along L direction, 12 mm along T (R) direction, and 5–7 mm along S (R) direction, where the T direction is perpendicular to the L and S direction of the plates. The direction and area of heat loading were L direction and 4 mm  $\times$  4 mm, respectively. The heat loaded surface was polished to an arithmetic mean surface roughness,  $R_a$ , of approximately 0.1  $\mu$ m.

The maximum surface temperatures during thermal shock tests can be predicted by the following equation [22];

$$\Delta T = 2P \left(\frac{t}{\pi \lambda \rho c}\right)^{0.5} \tag{1}$$

where  $\Delta T$ , P, t,  $\lambda$ ,  $\rho$ , and c are temperature change, absorbed energy density (0.19 or 0.38 GW/m<sup>2</sup>), heat load time (1 ms), thermal conductivity, density, and specific heat. By using this equation and experimental values of  $\lambda$ ,  $\rho$ , and c [17, 21], approximate maximum surface temperature was calculated to 1360 and 1730 °C under 0.19 and 0.38 GW/m<sup>2</sup> irradiations, respectively.

The post-mortem analyses to evaluate the damage caused by the thermal shock tests were carried out, which consisted of 1) observation of the damage of the heat loaded surface using a scanning electron microscope (SEM) and an optical microscope (OM), 2) evaluation of the crack distribution and length by observation from the cross-sectional surface along the heat loading direction using an OM, and 3) profilometry to measure the arithmetic mean roughness,  $R_a$ , of the heat loaded surface.

## 3. Results and discussion

Surface images after thermal shock tests are shown in Fig. 1. The cracks could be distinguished into two types; one is a micro crack with relatively short length (order of 10-100  $\mu$ m) and the other is a macro crack with relatively long length (order of millimeter).

Micro cracks of KW, W3R, and KW3R heat-loaded at 0.19 GW/m<sup>2</sup> and W3R and KW3R heat-loaded at 0.38 GW/m<sup>2</sup> were formed along the T direction. Considering the anisotropic grain structure and the lowest strength along the S direction of hot-rolled plates in the as-received condition, the micro cracks could be formed at the boundaries of layered grain structure by hot-rolling [19]. In contrast, micro cracks of PW, PW/Rxx, KW3R/Rxx, and KW/Rod heat-loaded at 0.19 GW/m<sup>2</sup> and PW, PW/Rxx, KW, KW3R/Rxx, and KW/Rod heat-loaded at 0.38 GW/m<sup>2</sup> were formed along non-particular directions. Considering no anisotropy in the grain boundary strength of the recrystallized materials and the rod materials along radial direction in the as-received condition, the micro cracks could be formed along the grain boundaries. The asreceived materials with relatively low  $T_{Rxx}$  and high DBTT (PW), as-received materials with relatively low strength and high DBTT (KW/Rod), and the recrystallized materials (PW/Rxx and KW3R/Rxx) with intrinsic low grain boundary strength and high DBTT showed micro cracks along the grain boundaries even under the low power density [18, 19]. In contrast, even under the heat load at 0.38 GW/m<sup>2</sup>, the W3R and KW3R with relatively high  $T_{Rxx}$  and low DBTT showed the micro cracks along the T direction. Based on these surface observations, the formation site of micro cracks in hot-rolled plate materials could be changed from the boundaries of layered grain structure to the grain boundaries, which might be caused by the progress of recrystallization resulting in the disappearance of the anisotropy in the grain boundary strength, decrease in the grain boundary strength, and increase in the DBTT. Although the KW/Rod has relatively high  $T_{\text{Rxx}}$ , the micro cracks formed at the grain boundaries even under the low power density, which might be attributed to the relatively low strength and high DBTT [18].

Macro cracks along T direction were only observed in the PW and KW3R under the heat load at  $0.38 \text{ GW/m}^2$ . Based on the experimental  $T_{\text{Rxx}}$  and the calculated maximum surface temperature, the recrystallization would progress rapidly in the PW under the heat load at  $0.38 \text{ GW/m}^2$ . Therefore, the macro cracks of PW could be formed by the coalescence of the microcracks along the grain boundaries after the recrystallization progressed. In contrast, the recrystallization would progress slowly in the KW3R. Therefore, the macro cracks of KW3R could be formed by the coalescence of the micro-cracks along the boundary of layered grain structure by hot-rolling before the recrystallization progressed. However, the reasons why macro cracks were formed only in these two materials are not clear at the moment. Further investigations to clarify the detailed mechanism of the micro and macro crack formation are planned as future work.

Evaluation of the crack depth by observation from the cross-sectional surface along the heat loading direction was conducted on the as-received materials, as shown in Fig. 2. Cracks with a lot of number below 80  $\mu$ m in depth were observed in all materials, which correspond to the micro cracks observed from the heat-loaded surface. In contrast, cracks with small number above 200  $\mu$ m in depth were observed only in the PW and KW3R, which correspond to the macro cracks observed from the heat-loaded surface. The number of the micro cracks and the depth of the deepest micro crack of the KW, W3R, and KW3R were smaller and shorter compared to the PW, respectively. In contrast, no significant difference of the number and depth of micro cracks between the PW and KW/Rod were observed. Based on these evaluations from the cross-sectional surfaces, the W materials with relatively high  $T_{\rm Rxx}$  and low DBTT, which were improved by the K-doping and alloying by Re, could show the suppressed formation of the micro cracks compared to the PW. Although the KW/Rod has relatively high  $T_{\rm Rxx}$  by the K-doping, no significant difference between the PW and KW/Rod could be observed because of the relatively low strength and high DBTT of the KW/Rod [18].

Fig. 3 shows the relationship between annealing temperature before thermal shock tests and surface roughness,  $R_a$ , produced by thermal shock tests. Under the heat load at 0.19 GW/m², the changes of  $R_a$  from the initial value (approximately 0.1  $\mu$ m) by thermal shock tests were very small except the PW/Rxx. In contrast, under the heat load at 0.38 GW/m²,  $R_a$  increased into approximately 1  $\mu$ m by thermal shock tests except the KW and KW/Rod, whose  $R_a$  were more than 2  $\mu$ m. According to the surface observation shown in Fig. 1, relatively large  $R_a$  of KW might be influenced by the roughened surface, while that of KW/Rod might be influenced by the widely-opened cracks because surface of this material was relatively smooth. Although the recrystallization influenced significantly on the  $R_a$  of several kinds of pure W reported by Pintsuk *et al* [23], no significant increase in  $R_a$  by recrystallization was observed in the PW and KW3R of the present study. Further investigations to clarify the correlation between the roughness change and material properties and effect of recrystallization are planned as future work.

# 4. Conclusion

Thermal shock behaviors under ELM-like heat load of the pure W, K-doped W, W-3%Re, and K-doped W-3%Re plates and K-doped W rod were investigated to clarify the effect of K-doping and alloying by Re. The results of this study were summarized as follows:

- 1) The cracks could be distinguished into two types; one is a micro crack with relatively short length and the other is a macro crack with relatively long length.
- 2) The formation site of micro cracks in hot-rolled plate materials could be changed from the boundaries of layered grain structure to the grain boundaries, which might be caused by the

- progress of recrystallization. The swaged rod material showed micro crack formation at the grain boundaries regardless of the test conditions.
- 3) The W materials with relatively high recrystallization temperature and low DBTT (K-doped W, W-3%Re, and K-doped W-3%Re plates), which were improved by the K-doping and alloying by Re, could show the suppressed formation of the micro cracks compared to the pure W. However, K-doped W-3%Re plate appeared to show small number of larger cracks than either K-doped W or W-3%Re plates.

# 5. Acknowledgments

This work was performed under the IEA technology collaboration program of plasma wall interaction (PWITCP) and financially supported by the National Institute for Fusion Science (NIFS) and JSPS KAKENHI Grant Number 15KK0224, Japan.

#### References

- [1] Pintsuk G *et al* 2013 Qualification and post-mortem characterization of tungsten mock-ups exposed to cyclic high heat flux loading *Fus. Eng. Des.* **88** 1858–1861
- [2] Nogami S *et al* 2017 Degradation of Tungsten Monoblock Divertor under Cyclic High Heat Flux Loading *Fus. Eng. Des.* **120** 49–60
- [3] Seki Y *et al* 2016 A study of plasma facing tungsten components with electrical discharge machined surface exposed to cyclic thermal loads *Fus. Eng. Des.* **109–111** 1148–1152
- [4] Chebotarev V V *et al* 1996 Characteristics of transient plasma layers produced by irradiation of graphite targets by high power quasi-stationary plasma streams under the disruption simulation conditions *J. Nucl. Mater.* **233–237** 736–740
- [5] Temmerman G De *et al* 2013 High heat flux capabilities of the Magnum-PSI linear plasma device *Fus. Eng. Des.* **88** 483–487
- [6] Linke J *et al* 1995 Evaluation of cooling concepts and specimen geometries for high heat flux tests on neutron irradiated divertor elements *Fus. Eng. Des.* **28** 72–80
- [7] Majerus P *et al* 2005 The new electron beam test facility JUDITH II for high heat flux experiments on plasma facing components *Fus. Eng. Des.* **75–79** 365–369
- [8] Farrell K *et al* 1967 Recrystallization, grain growth and the ductile-brittle transition in tungsten sheet *J. Less-Common Met.* **13** 141–155
- [9] Wei Q *et al* 2008 Effect of low-temperature rolling on the tensile behavior of commercially pure tungsten *Mater. Sci. Eng.* **A 491** 62–69
- [10] Luo A *et al* 1991 Ultrahigh temperature tensile properties of arc-melted tungsten and tungsten-iridium alloys *Scr. Metall.* **25** 2411–2414
- [11] Schade P 2010 100years of doped tungsten wire Int. J. Refract. Met. Hard Mater. 28 648-

660

- [12] Coenen J W *et al* 2017 Advanced materials for a damage resilient divertor concept for DEMO: Powder-metallurgical tungsten-fibre reinforced tungsten *Fus. Eng. Des.* **124** 964–968
- [13] Reiser J et al 2017 Ductilisation of tungsten (W): Tungsten laminated composites Int. J. Refract. Met. Hard Mater. 69 66–109
- [14] Nogami S *et al* 2019 A review of impact properties of tungsten materials *Fus. Eng. Des.* **141** 48–61
- [15] Nogami S *et al* 2018 Improvement of impact properties of tungsten by potassium doping *Fus. Eng. Des.* **135** 196–203
- [16] Tsuchida K *et al* 2018 Recrystallization behavior of hot-rolled pure tungsten and its alloy plates during high-temperature annealing *Nucl. Mater. Energy* **15** 158–163
- [17] Nogami S *et al* 2017 Feasibility of utilizing tungsten rod for fusion reactor divertor *Fus. Sci. Tech.* **72** 673–679
- [18] Nogami S et al 2016 Effect of microstructural anisotropy on the mechanical properties of K-doped tungsten rods for plasma facing components Fus. Eng. Des. 109–111 1549–1553
- [19] Fukuda M *et al* 2015 Anisotropy in the mechanical properties of potassium and rhenium doped tungsten alloy plates for fusion reactor applications, *Fusion Sci. Technol.* **68** 690–693
- [20] Fukuda M et al 2014 Tensile properties of K-doped W-3%Re Fus. Eng. Des. 89 1033–1036
- [21] Fukuda M *et al* 2018 Thermal properties of pure tungsten and its alloys for fusion applications *Fus. Eng. Des.* **132** 1–6
- [22] Oosterkamp W J 1948 The heat dissipation in the anode of an X-ray tube *Philips Research Reports* **3** 49–59
- [23] Pintsuk G *et al* 2018 Recrystallization and composition dependent thermal fatigue response of different tungsten grades *Int. J. Refract. Met. Hard Mater.* **72** 97–103

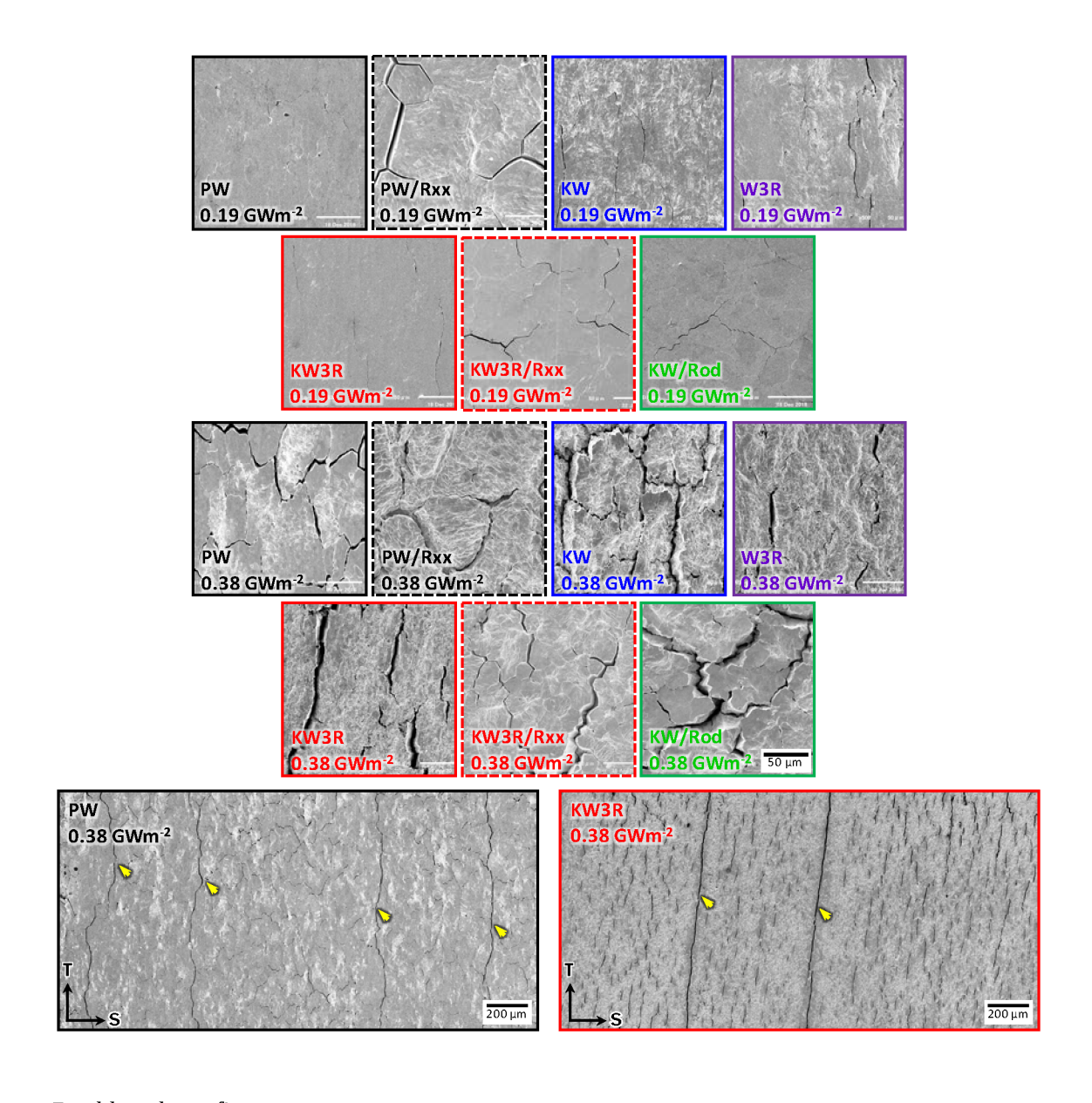
Table 1 Summary of material information (major chemical composition, heat treatment condition, abbreviation of material name, grain size ( $d_S$  and  $d_R$ ) [14–20], recrystallization temperature ( $T_{Rxx}$ ) [16], tensile strength ( $\sigma_S$  and  $\sigma_R$ ) [18, 19], DBTT by tensile test (DBTT<sub>tens</sub>) [18, 19], and IPF image obtained by an EBSD).

Material	Pure W (Plate)		K-doped W (Plate)	W-3%Re (Plate)	K-doped W-3%Re (Plate)		K-doped W (Rod)
Heat-treatment condition	As-received	Re- crystallized	As-received	As-received	As-received	Re- crystallized	As-received
Abbreviation	PW	PW/Rxx	KW	W3R	KW3R	KW3R/Rxx	KW/Rod
$d_{\mathrm{S}},d_{\mathrm{R}}\left[\mu\mathrm{m} ight]$	22	200–600	11	19	8	74	50
$T_{ m Rxx}$	1200	-	1300	1500	1500	_	1500
$\sigma_{\rm S}, \sigma_{\rm R}$ [MPa]	~400	Not tested	~400	~400	~400	Not tested	~300
DBTT <sub>tens</sub> [°C]	700	Not tested	500	500	500	Not tested	700
IPF image	S 1 50 μm	S 50 μm	S 50 μm	S 50 μm	S 50 μm	\$5 <u>0 μ</u> m	R 50 μm

- As-received condition is a condition just after stress-relief heat treatment.
- L, S, and R directions correspond to the rolling (swaging) direction of the plate (rod), direction along thickness of the plate, and radial direction of the rod, respectively.
- $d_S$ ,  $d_R$ : Grain size along thickness of the plates and along diameter of the rod
- $T_{\text{Rxx}}$ : Recrystallization temperature based on the Vickers hardness
- $\sigma_S$ ,  $\sigma_R$ : Tensile strength at 1000 °C along S direction of the plates and along R direction of the rod
- DBTT<sub>tens</sub>: DBTT by tensile test along S direction of the plates and along R direction of the rod
- $\bullet \;\; IPF$  image obtained by an EBSD of L × S surface of the plates and L × R surface of the rod

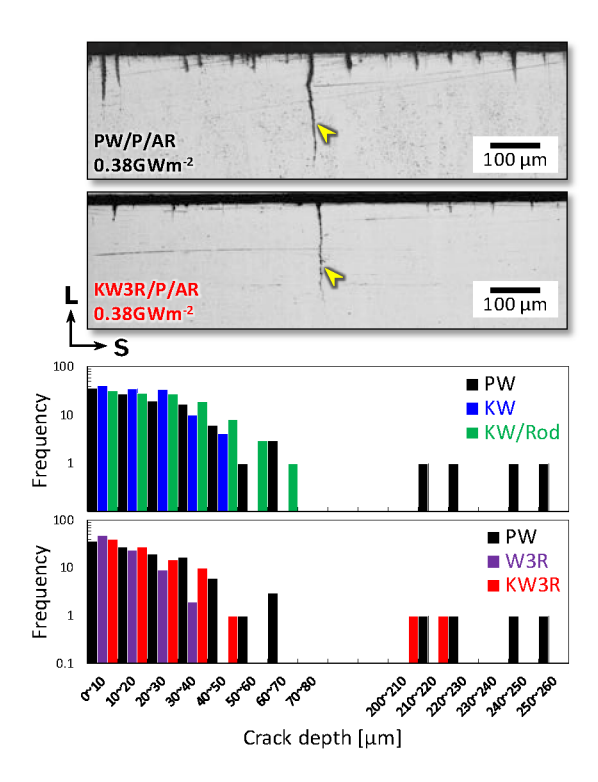
Double column figure

Fig. 1 Surface images after thermal shock tests obtained by an SEM of PW, PW/Rxx, KW, W3R, KW3R, KW3R/Rxx, and KW/Rod ( $T \times S$  surfaces for the plates and radial surface for the rod). The yellow arrows indicate the macro cracks.



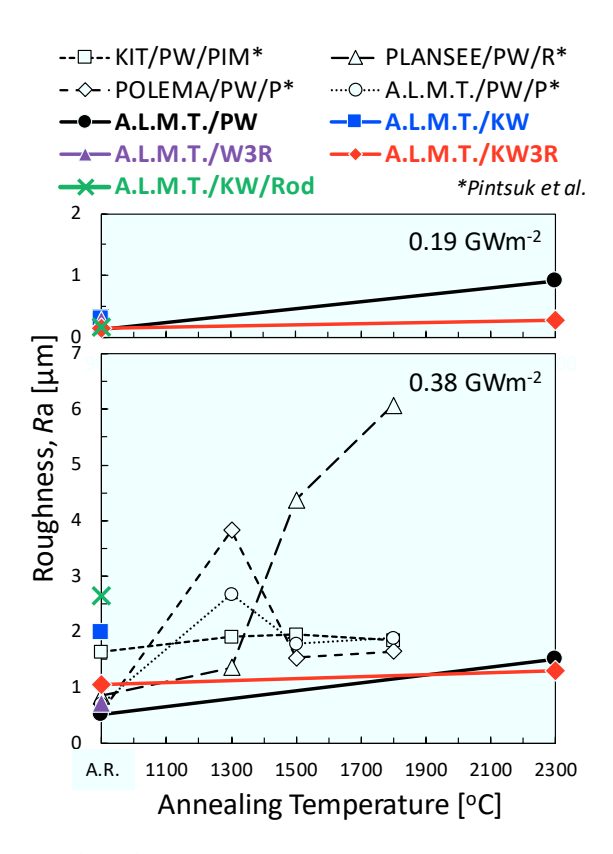
Double column figure

Fig. 2 Cross-sectional images after thermal shock tests obtained by an OM of PW and KW3R and histogram of crack depth measured using the cross-sectional images of PW, KW, W3R, KW3R, and KW/Rod. The yellow arrows indicate the macro cracks.



Single column figure

Fig. 3 Relationship between annealing temperature before thermal shock tests and surface roughness produced by thermal shock tests of PW, KW, W3R, KW3R, and KW/Rod. Roughness data of four kinds of pure W reported by Pintsuk *et al.* [23] are also plotted.



Single column figure